Applied Catalysis A: General 454 (2013) 81–87

Contents lists available at SciVerse ScienceDirect

Applied Catalysis A: General

journal homepage: www.elsevier.com/locate/apcata

C_2-oxygenates synthesis through CO hydrogenation on SiO_2-ZrO_2 supported Rh-based catalyst: The effect of support

Lupeng Han, Dongsen Mao*, Jun Yu, Qiangsheng Guo, Guanzhong Lu

Research Institute of Applied Catalysis, School of Chemical and Environmental Engineering, Shanghai Institute of Technology, Shanghai 201418, PR China

ARTICLE INFO

Article history:
Received 14 October 2012
Received in revised form 6 January 2013
Accepted 8 January 2013
Available online xxx

Keywords:
Syngas
C_2-oxygenates
Rh-based catalyst
SiO_2-ZrO_2 mixed oxide

ABSTRACT

Rh-Mn-Li catalysts supported on SiO_2, ZrO_2 and SiO_2-ZrO_2 mixed oxides with various molar ratios of Si/Zr were prepared and tested for the synthesis of C_2-oxygenates from syngas. Compared with pure SiO_2 and ZrO_2 supported catalysts, catalysts supported on SiO_2-ZrO_2 mixed oxides showed higher activity and C_2-oxygenates selectivity, in which Rh-Mn-Li/SiO_2-ZrO_2 (molar ratio of Si/Zr = 1:3) exhibited the best yield of C_2-oxygenates. The effect of the support on the performance of the Rh-based catalysts was investigated comprehensively by XRD, N_2 adsorption-desorption, H_2 and CO uptakes, FT-IR, XPS, H_2-TPR, TPSR and CO-TPD techniques. The results indicated that the chemical state of Rh, CO adsorption species, dispersion of Rh and the ability of CO hydrogenation varied over catalysts supported on SiO_2, ZrO_2 and SiO_2-ZrO_2 mixed oxides, which led to the diverse catalytic activity toward C_2-oxygenates synthesis.

1. Introduction

As increasing awareness of global climate change and of the energetic dependence on petroleum, a novel technology for the production of C_2-oxygenates such as ethanol, acetic acid and acetaldehyde from syngas has attracted more attention worldwide. As well known, supported Rh-based catalysts exhibit predominant performance for the synthesis of C_2-oxygenates from hydrogenation of CO [1–4]. Extensive research on the effects of promoters and supports has been devoted to improve activity and selectivity toward the formation of C_2-oxygenates. Rh-based catalysts promoted with promoters, such as Mn, Li, Fe, Ti, Zr, La, Sm, V, could notably increase the activity and selectivity toward target products [5–12]. Previous work on supports has been concentrated principally on SiO_2 due to its high surface area, ample porosity and good stability [13–15]. However, other supports, such as oxides of Ti, Ce, V, Nb, Zr, have been reported to be more favorable for the formation of C_2-oxygenates [7,16–19]. Very recently, we found that Rh-Mn-Li catalyst supported on SiO_2-TiO_2 mixed oxide exhibited better activity and C_2-oxygenates selectivity than that on pure SiO_2 and TiO_2 [20]. On the other hand, the oxide of Zr as an oxophilic promoter, like Fe, Mn, Ti, could improve the catalytic activity toward C_2-oxygenates, in which the rational mechanism has been suggested by Wang et al. [9]. Based on the above results, Rh catalysts supported on SiO_2-ZrO_2 mixed oxide may also promote the formation of C_2-oxygenates, which has not been reported hitherto, to the best of our knowledge.

In the present study, SiO_2-ZrO_2 mixed oxides with various molar ratios, used as supports for Rh catalysts promoted by Mn and Li, were prepared, aiming at improving the catalytic performance for the synthesis of C_2-oxygenates from CO hydrogenation. As comparison, Rh-based catalysts supported on pure SiO_2 and ZrO_2 were also prepared and tested. The effect of support on performance of Rh-based catalysts was characterized comprehensively by X-ray powder diffraction (XRD), N_2 adsorption-desorption, H_2 and CO uptakes, X-ray photoelectron spectroscopy (XPS), Fourier transform infrared (FT-IR) spectroscopy, H_2 temperature-programmed reduction (H_2-TPR), temperature-programmed surface reaction (TPSR) and temperature-programmed desorption (TPD) of chemisorbed CO.

2. Experimental

2.1. Catalyst preparation

(1) SiO_2-ZrO_2 mixed oxides with Si/Zr molar ratios of 1:1, 1:3 and 1:9 were prepared by conventional impregnation method [21,22] with commercial SiO_2 (Qingdao Ocean Desiccant Co., P.R. China) and $Zr(NO_3)_4{\cdot}5H_2O$ (SCRC). Firstly, SiO_2 was boiled in de-ionized water for 24 h and then dried at 90 °C for 12 h to remove the surface impurities. 10 g $Zr(NO_3)_4{\cdot}5H_2O$ was added into a suitable amount of de-ionized water to form a uniform solution under rapid stirring. Then, a certain amount of SiO_2 (based on the molar ratio of Si/Zr) was added into the solution to the incipient wetness.

* Corresponding author. Tel.: +86 21 60877221; fax: +86 21 60877231.
E-mail addresses: dsmao@sit.edu.cn, dsmao1106@yahoo.com.cn (D. Mao).

0926-860X/$ – see front matter © 2013 Elsevier B.V. All rights reserved.
http://dx.doi.org/10.1016/j.apcata.2013.01.008

The paste was dried at 90 °C for 24 h and then calcined in static air at 500 °C for 4 h. (2) SiO_2 support was also prepared from commercial SiO_2 and treated with the same method as described above except the addition of zirconium nitrate was omitted. (3) ZrO_2 support was prepared from $Zr(NO_3)_4{\cdot}5H_2O$ that was calcined in static air at 500 °C for 4 h.

$RhCl_3$ hydrate (Rh ~ 36 wt%, Fluka), $Mn(NO_3)_2$ solution (50%, SCRC), $LiNO_3$ (99.99%, SCRC) and the supports mentioned above were used in catalyst preparations. All the catalysts were prepared by the incipient wetness impregnation method, and Rh loading was 2 wt% and the weight ratio of Rh:Mn:Li = 2:2:0.05. Impregnated catalysts were dried at 90 °C for 8 h and subsequently calcined in static air at 350 °C for 4 h. The obtained catalysts are denoted as RML/SiO_2, RML/SZ(1:1), RML/SZ(1:3), RML/SZ(1:9) and RML/ZrO_2, respectively.

2.2. Catalyst testing

CO hydrogenation was performed in a fixed-bed micro-reactor with length of ~350 mm and internal diameter of ~5 mm. The catalyst (0.3 g) was loaded between quartz wool and axially centered in the reactor tube, with the temperature monitored by a thermocouple close to the catalyst bed. Prior to reaction, the catalyst was heated to 400 °C (heating rate ~3 °C/min) and reduced with H_2/N_2 (50 mL/min, $V(H_2)/V(N_2) = 1{:}9$) for 2 h at atmospheric pressure. The catalyst was then cooled down to 280 °C and the reaction started as gas flow was switched to a H_2/CO mixture (50 mL/min, $V(H_2)/V(CO) = 2{:}1$) at 3 MPa. All post-reactor lines and valves were heated to 150 °C to prevent product condensation. The products were analyzed for both oxygenates and hydrocarbons on-line by Agilent GC 6820 equipped with a FID (flame ionization detector) and a TCD (thermal conductivity detector). The conversion of CO was calculated based on the fraction of CO that formed carbon-containing products according to: %Conversion = $(\sum n_i M_i / M_{CO}) \times 100$, where n_i is the number of carbon atoms in product i, M_i is the percentage of product i detected, and M_{CO} is the percentage of CO in the syngas feed. The selectivity of a certain product was calculated based on carbon efficiency using the formula $\%S_i = (n_i C_i / \sum n_i C_i) \times 100$, where n_i and C_i are the carbon number and molar concentration of the ith product, respectively.

2.3. Catalyst characterization

XRD patterns were recorded on a PANalytical X'Pert instrument using Ni filtered Cu Kα radiation ($\lambda = 0.15418$ nm) at 40 kV and 40 mA. Two theta angles ranged from 10° to 80° with a scanning rate of 6° per minute.

N_2 adsorption-desorption isotherms were obtained at −196 °C on a Micromeritics ASAP 2020 M + C adsorption apparatus, after all samples were degassed under vacuum at 200 °C for 3 h. BET surface areas were calculated from the linear part of the BET plot.

The H_2 uptakes of various catalysts were calculated on the basis of H_2-TPD profiles. For H_2-TPD measurements, the catalyst (0.1 g) was reduced in situ for 2 h at 400 °C in 10% H_2/N_2 (50 mL/min), and then was held at 400 °C for another 30 min before being cooled down to room temperature (RT) in He flow. The next step was H_2 adsorption at RT for 0.5 h, and then the gas was swept again with He for 3 h. Subsequently, the sample was heated in a flowing He stream (50 mL/min) up to ~650 °C at a rate of 10 °C/min, while the desorbed species was detected with a TCD detector.

The CO uptakes of various catalysts were measured by pulse adsorption of CO using a quadrupole mass spectrometer (QMS, Balzers OmniStar 200). The catalyst (0.2 g) was reduced for 2 h at 400 °C in H_2/He (50 mL/min, $V(H_2)/V(He) = 1{:}9$), and then was held at 400 °C for another 30 min before being cooled down to room temperature (RT) in He flow. The amount of chemisorbed CO was measured by injecting CO (>99.97%) into the He carrier gas in pulse mode.

XPS spectra were recorded by a Kratos AXIS ULTRADLD X-ray photoelectron spectrometer using Al-Kα (1486.6 eV) as the exciting source. The C 1s (284.9 eV) was used as an internal standard. In these experiments, the samples were reduced with H_2/N_2 (50 mL/min, $V(H_2)/V(N_2) = 1{:}9$) at 400 °C for 2 h before measurement. Rhodium peaks were decomposed into several components assuming that the peaks had Gaussian-Lorentzian shapes. The percentage of Rh^0 and Rh^+ was calculated on the basis of peak area respectively.

CO adsorption was studied using a Nicolet 6700 FT-IR spectrometer equipped with a DRIFT (diffuse reflectance infrared Fourier transform) cell with CaF_2 windows. The sample in the cell was pretreated in H_2/N_2 (50 mL/min, $V(H_2)/V(N_2) = 1{:}9$) at 400 °C for 2 h, followed by N_2 (50 mL/min, Ultrahigh-purity) flushing at 400 °C for 0.5 h. After temperature was dropped to 280 °C and 50 °C, the background was scanned in N_2, respectively. Followed by introducing 1% CO/N_2 (50 mL) into the IR cell, the IR spectrum of CO adsorbed on the catalyst was recorded at 50 °C and 280 °C respectively, when adsorption state remained steady. The concentration of CO was higher than 99.97% and it was pretreated by dehydration and deoxygenization before use. The spectral resolution was 4 cm^{-1} and the scan times were 64.

H_2 temperature-programmed reduction (TPR) was carried out in a quartz microreactor. Firstly, 0.1 g of the as-prepared sample was pretreated at 350 °C in N_2 for 1 h prior to a TPR measurement. During the TPR experiment, H_2/N_2 mixture gas with $V(H_2)/V(N_2) = 1{:}9$ was used at 50 mL/min and the temperature was ramped from RT to 500 °C at 10 °C/min while the effluent gas was analyzed with a TCD.

The temperature-programmed surface reaction (TPSR) and temperature-programmed desorption (TPD) of chemisorbed CO experiments were carried out as follows: after the catalyst was reduced at 400 °C in H_2/N_2 (50 mL/min, $V(H_2)/V(N_2) = 1{:}9$) for 2 h, it was cooled down to RT and CO was introduced for adsorption for 0.5 h; afterwards, the H_2/N_2 mixture or He was swept again, and the temperature was increased to 650 °C at the rate of 10 °C/min with a quadrupole mass spectrometer (QMS, Balzers OmniStar 200) as the detector to monitor the signals of CH_4 ($m/z = 15$) and CO ($m/z = 28$), respectively.

3. Results and discussion

3.1. CO hydrogenation performance of the catalysts

Table 1 shows the performance of CO hydrogenation at 280 °C on all the catalysts investigated. As observed, C_2-oxygenates selectivity improved notably over the catalysts supported on ZrO_2 and SiO_2-ZrO_2 mixed oxides, compared with RML/SiO_2, indicating that ZrO_2 as support indeed could boost the formation of C_2-oxygenates, which has been reported previously by Ichikawa [23]. On the other hand, catalysts supported on SiO_2-ZrO_2 mixed oxides showed improved catalytic activity (CO conversion) than that over pure SiO_2 and ZrO_2 supported catalysts, in which RML/SZ(1:3) exhibited the highest CO conversion of 3.9%, increasing by ca. 50% compared with RML/SiO_2 and RML/ZrO_2. Moreover, the yield of C_2-oxygenates increased in the following order: RML/SiO_2 < RML/ZrO_2 < RML/SZ(1:9) < RML/SZ(1:1) < RML/SZ(1:3), in which the maximum of 71.3 g/(kg·h) was attained over RML/SZ(1:3), which was more than three times of that on the RML/SiO_2 catalyst (23.6 (g/(kg h)).

Table 1
CO hydrogenation performance on different catalysts.

Catalyst	CO Conv. (%)	Selectivity of products (%)							STY of C_2-oxy (g/(kg·h))
		CO_2	CH_4	MeOH	HAc	EtOH	C_2^+HC[a]	C_2-oxy[b]	
RML/SiO_2	2.6	10.5	10.4	2.4	10.6	21.4	44.6	32.1	23.6
RML/SZ(1:1)	3.3	4.6	14.1	0.7	38.5	20.2	21.9	58.7	52.7
RML/SZ(1:3)	3.9	4.1	11.2	0.5	50.0	16.0	18.2	66.0	71.3
RML/SZ(1:9)	2.9	5.3	9.0	0.6	48.0	18.4	18.8	66.4	52.5
RML/ZrO_2	2.7	8.5	7.1	0.6	32.8	29.0	22.0	61.8	45.8

Reaction conditions: t = 280 °C, p = 3 MPa, SV = 10,000 mL/(g h), $V(H_2)/V(CO)$ = 2, data taken after 13 h when reaction state remains steady.
[a] C_2^+HC denotes hydrocarbons containing two and more carbon atoms.
[b] C_2-oxy denotes oxygenates containing two and more carbon atoms.

3.2. XRD and N_2 adsorption results

Fig. 1 shows the XRD patterns of different catalysts after calcination at 350 °C for 4 h. As seen, a very broad peak at 2θ of ~23° was clearly observed on RML/SiO_2, which can be ascribed to amorphous SiO_2. On the other hand, a very weak and broad peak at 2θ of ~37°, which can be assigned to Rh_2O_3 phase [24], was also observed (see inset of Fig. 1). After reduction in H_2 at 400 °C for 4 h, the diffraction peak ascribed to Rh_2O_3 phase disappeared; and a broad peak at 2θ of ~42° which was attributed to the (1 1 1) plane of Rh metal [25], was seen, indicating the reduction of Rh_2O_3 to Rh.

On the other hand, the diffraction peaks of both monoclinic zirconia (m-ZrO_2, JCPDS 83-0940) and tetragonal zirconia (t-ZrO_2, JCPDS 88-1007) appeared on ZrO_2 and SiO_2-ZrO_2 supported catalysts. Moreover, it can be found that the diffraction peaks of ZrO_2 become stronger and sharper, with increase of the amount of ZrO_2 in the support, indicating that a continuous increase in the crystallization degree of ZrO_2 when the amount of ZrO_2 increased. It should be emphasized that the presence or not of Rh_2O_3 phase and metallic Rh on ZrO_2 and SiO_2-ZrO_2 supported catalysts cannot be judged, since the diffraction lines from Rh_2O_3 and Rh may be overlapped with the strong ZrO_2 diffraction lines. For that reason the XRD spectra of ZrO_2 and SiO_2-ZrO_2 supported catalysts after reduction in H_2 were not presented here.

As shown in Table 2, the surface area of catalysts decreases sequentially with the increase of amount of ZrO_2 in support, i.e. the RML/SiO_2 has the largest one and the RML/ZrO_2 has the smallest one. Combing the results of activity testing (Table 1) and N_2 adsorption characterization (Table 2), it can be seen that, though the surface area of RML/SiO_2 is the biggest, both CO conversion and C_2-oxygenates selectivity over it are the poorest. However, RML/SZ(1:3) with medium surface area owns the best catalytic activity toward C_2-oxygenates. The result indicates that the textural characteristics of the catalysts are not directly related to their catalytic performance, which was also obtained previously by us [20,26,27] and other researchers [28,29].

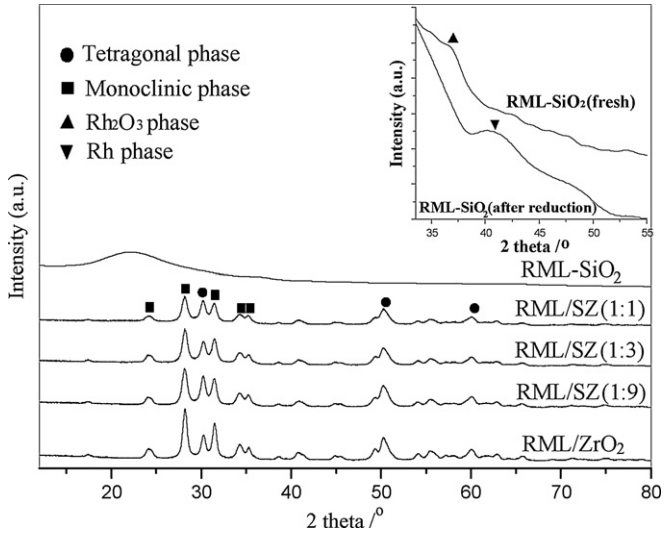

Fig. 1. XRD profiles of different catalysts.

3.3. H_2 and CO uptakes results

The results of H_2 and CO uptakes on various catalysts are also listed in Table 2. As shown, both chemisorbed H_2 and CO first increased and then decreased with increasing amount of ZrO_2 in the supports. The decrease of chemisorbed H_2 and CO may be due to Rh surface partially covered by the reduction species of ZrO_2. Some researchers [30,31] have also reported that reduction species of ZrO_2 could migrate over Rh surface during thermal pretreatment in H_2 stream, which led to the decrease of chemisorbed CO and H_2. As the amount of chemisorbed H_2 and CO could reflect the Rh dispersion to a degree, the Rh dispersion of the catalysts increase in the order of RML/SiO_2 < RML/ZrO_2 < RML/SZ(1:9) < RML/SZ(1:1) < RML/SZ(1:3), which is in line with the catalytic activity of the catalysts.

On the other hand, it can be seen from Table 2 that compared with RML/SiO_2 and RML/ZrO_2, SiO_2-ZrO_2 supports decrease Rh particle size to some degree, in which the particle size in RML/SZ(1:3) was the smallest (4 nm), which is a suitable size for the synthesis of C_2-oxygenates from syngas over Rh-based catalysts [17,32].

3.4. FT-IR study

Fig. 2 shows IR spectra of CO adsorbed on different catalysts recorded at 50 °C. According to the literature [10,14], there are mainly three CO adsorption states on Rh particle: geminal CO formed on the Rh^+ sites, with characteristic absorption bands at ca. 2100 and 2030 cm^{-1}; linear CO on Rh^0 sites with absorption band at ca. 2060 cm^{-1} and bridged CO on Rh^0 sites with a broad absorption band at ca. 1860 cm^{-1}. As shown in Fig. 2, geminal CO could be observed on all the catalysts; however, linear CO could only be observed on RML/SiO_2 and RML/SZ(1:1), and no noticeable bridged CO was observed on all the catalysts. Furthermore, linear CO disappeared when the amount of ZrO_2 dominated in the

Table 2
Specific surface areas, H_2 and CO uptakes and Rh particle size of different catalysts.

Catalyst	S_{BET} (m^2/g)	H/Rh (molar ratio)	CO/Rh (molar ratio)	d_{Rh} [a] (nm)
RML/SiO_2	347.9	0.17	0.18	7.5
RML/SZ(1:1)	127.2	0.27	0.35	4.7
RML/SZ(1:3)	92.5	0.32	0.40	4.0
RML/SZ(1:9)	51.9	0.25	0.34	5.1
RML/ZrO_2	41.3	0.20	0.29	6.3

[a] Rh particle size was calculated from the equation $d = 5/S\,\rho$, where S is the metal surface area and ρ is the density of the metal, assuming that hydrogen is essentially adsorbed by the Rh atoms with a stoichiometry of Rh_s:H = 1:1.

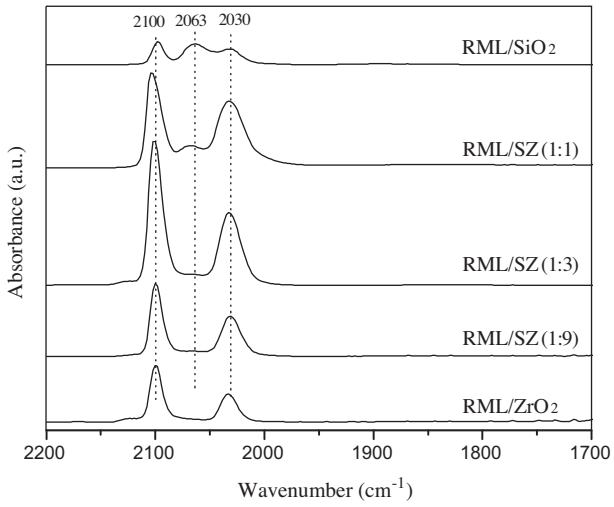

Fig. 2. IR spectra of CO chemisorbed on different catalysts for 80 min (steady state) at 50 °C.

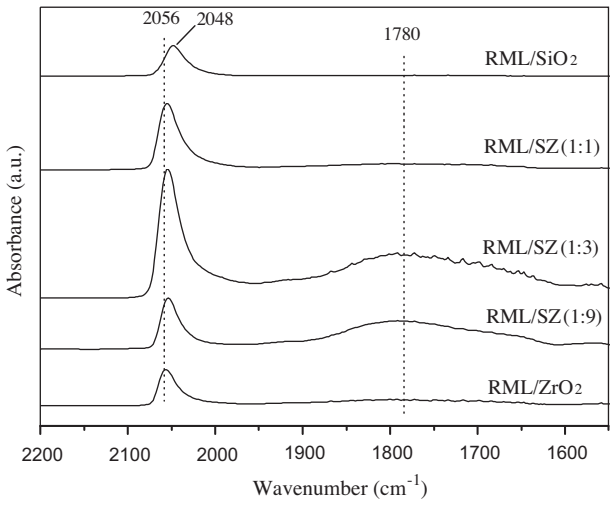

Fig. 3. IR spectra of CO chemisorbed on different catalysts for 10 min (steady state) at 280 °C.

support, indicating that ZrO_2 as support could stabilize Rh^+ ions and favor the formation of geminal CO. Some authors [5,33] have proposed that oxophilic promoters, such as oxide of Mn and Ti could suppress the reduction of rhodium, so more Rh^+ ions would exist on the catalyst surface. It is universally acknowledged that Rh^0 is the active center for CO dissociation, and Rh^+ sites are responsible for CO insertion to form intermediates of C_2-oxygenates [34–36]. Thus, more Rh^+ sites imply more activity sites for CO insertion, which could improve the selectivity toward C_2-oxygenates, based on the well-known C_2-oxygenates formation mechanism [37]. For this reason, catalysts supported on ZrO_2 and SiO_2-ZrO_2 mixed oxides especially SZ(1:3) and SZ(1:9) exhibit higher selectivity toward C_2-oxygenates than SiO_2 supported catalyst.

On the other hand, it is worthy to note that the intensity of geminal CO adsorption increases in the order of RML/SiO_2 < RML/ZrO_2 < RML/SZ(1:9) < RML/SZ(1:1) < RML/SZ(1:3), which implies that the dispersion of Rh on catalysts increases in the same order [38], which is in excellent line with the result from H_2 and CO uptakes measurements. According to literature [39,40], high dispersion of Rh suggests less formation of large Rh atom ensembles on the catalyst surface that is required for the dissociation of CO. Less dissociation of CO is thought to decrease the surface carbon coverage, resulting in increased H_2 chemisorption which is necessary for high activity and selectivity to oxygenates.

Fig. 3 shows IR spectra of CO adsorbed on different catalysts recorded at the reaction temperature of 280 °C. In comparison with the spectra recorded at 50 °C (Fig. 2), three changes can be observed obviously:

(1) The geminal CO disappeared in all the spectra. The disappearance of geminal CO may be caused by the reduction of $Rh^+(CO)_2$ to form CO_2 and $Rh_x^0(CO)$ species [10,12].
(2) Linear CO appeared in all the spectra at 2048–2056 cm^{-1}, and there was a shift to lower wave numbers, which can be due to the decrease in coverage [40]. On the other hand, the bands on catalysts supported on ZrO_2 and SiO_2-ZrO_2 mixed oxides shifted to a higher wave number, compared with that on catalyst supported on SiO_2. This shift may imply that the electron density of surface Rh decrease, leading to the formation of cationic Rh sites [41]. As pointed out above, cationic Rh sites are more active for CO insertion than reduced Rh sites, leading to higher selectivity to C_2-oxygenates.
(3) Another band at around 1780 cm^{-1} could be observed in all spectra except for RML/SiO_2. This feature band could not be attributed to bridged adsorbed CO, because its vibrational frequency was much lower than that of bridged adsorbed CO. This feature band may be attributed to a weakening of the C-O bond. Similarly, a band at around 1760 cm^{-1} was observed on Rh-Mn-Li/TiO_2 catalyst at 270 °C by Schwartz [42], who attributed this feature band to a substantial weakening of the C—O bond for the attractive electron action of oxophilic promoters. The weakening of the C—O bond contributes to CO dissociation, so better activity could be obtained [42]. As found that, adsorption amount of CO, especially the new adsorbed CO species, increased in the order: RML/SiO_2 < RML/ZrO_2 < RML/SZ(1:9) < RML/SZ(1:1) <RML/SZ(1:3), thus CO conversion of catalysts increased in the same order ineluctably.

3.5. XPS Study

The chemical state of the catalyst components and their relative abundance at the catalyst surface has been investigated by XPS after *in situ* reduction and the results are listed in Table 3. Moreover, the Rh 3d core level spectra of three representative catalysts are displayed in Fig. 4. From Fig. 4, it can be found that the BE of Rh $3d_{5/2}$ of RML/SiO_2 centered at 307.5 eV, indicating that Rh^0 is the major Rh species on the RML/SiO_2 catalyst. On the other hand, the BE of Rh $3d_{5/2}$ of catalysts supported on SiO_2-ZrO_2(1:3) and ZrO_2 centered at 308.4 eV, indicating that Rh^+ is the major Rh species on the catalysts containing ZrO_2 [43]. After curve fitting, the estimated percentage of Rh^0 and Rh^+ is given in parentheses and the ratio of Rh^+/Rh^0 increased in the order: RML/SiO_2 < RML/ZrO_2 < RML/SZ(1:3). These results are well in line with those from FT-IR measurements, which further confirmed that ZrO_2 and SiO_2-ZrO_2 as support could

Table 3
Binding energies (eV) of core electrons of different catalysts.

Catalyst	Binding energy (eV)			
	Rh $3d_{5/2}$[a]	Mn $2p_{3/2}$	Li 1s	Zr $3d_{5/2}$
RML/SiO_2	307.5 (77) 308.4 (23)	642.2	53.3	–
RML/SiO_2-ZrO_2(1:3)	307.5 (7) 308.4 (93)	642.3	53.6	182.6
RML/ZrO_2	307.4 (16) 308.5 (84)	641.9	53.1	182.0

[a] The data in parentheses represent the estimated percentage of each species.

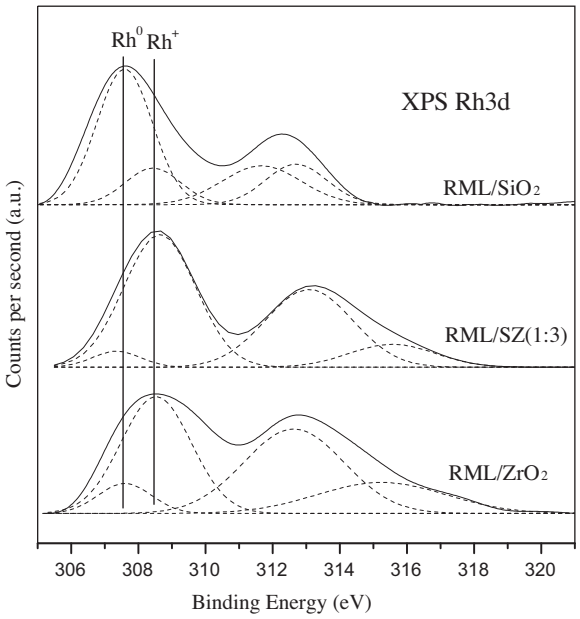

Fig. 4. XPS spectra of three representative catalysts.

stabilize Rh^+ ions. From the BEs of Mn $2p_{3/2}$, Li 1s and Zr $3d_{5/2}$, we know that Mn exists as Mn^{2+} or higher valence state (Mn^{3+} or Mn^{4+}), Li exists as Li^+ and Zr existes as Zr^{4+} at the catalyst surface [9].

3.6. H_2-TPR study

Fig. 5 shows the TPR profiles of different catalysts. It can be seen that there are three peaks (α, β and γ) of H_2 consumption on all samples except RML/SiO_2. The first two peaks (α, β) could be ascribed to the reduction of Rh_2O_3 not intimately contacting with Mn species and Rh_2O_3 intimately contacting with Mn species; and the third one (γ) could be ascribed to the reduction of Mn species [44]. However, there are only two peaks of H_2 consumption on RML/SiO_2. The similar observation for Rh-Mn/SiO_2 sample has also been reported by Chen et al. [33], who ascribed the β peak to the reduction of Rh-Mn species, where they had strong interaction. Since SiO_2 is an inert support, the interaction between Rh and Mn gets strong, which makes reduction peak of Mn species

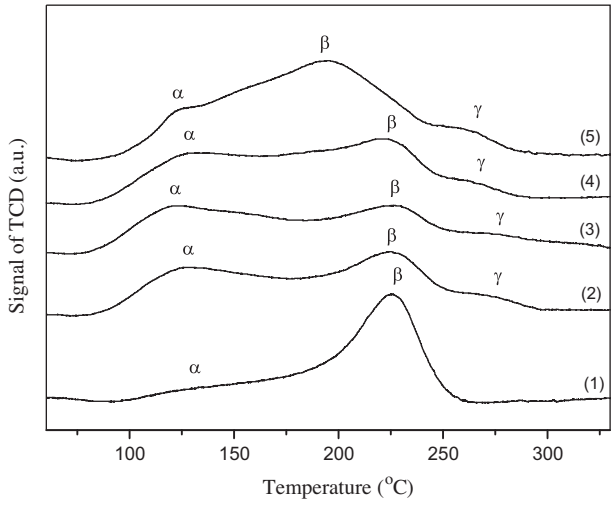

Fig. 5. H_2-TPR profiles of different catalysts. (1) RML/SiO_2, (2) RML/SZ(1:1), (3) RML/SZ(1:3), (4) RML/SZ(1:9), (5) RML/ZrO_2.

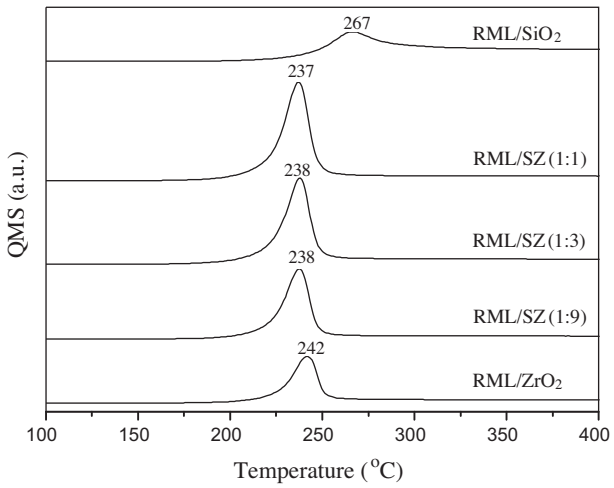

Fig. 6. TPSR profiles of different catalysts for CH_4 formation.

overlap with that of Rh_2O_3 intimately contacting with Mn species. However, ZrO_2 as a strong metal-support interaction support could interact with Rh and Mn, which weakened the strength of Rh-Mn interaction. Thus the reduction peak of Mn species was separated from the β peak over the catalysts supported on ZrO_2-containg carriers.

It has been reported that the geometrical structure of the active site for the formation of C_2-oxygenates is ($Rh_x{}^0Rh_y{}^+$)–O–M^{n+} (M = Mn or Zr, $2 \leq n \leq 4$), wherein a part of Rh is present as Rh^+ and the M^{n+} is in close contact with these Rh species [9]. The results from FT-IR and XPS indicate that plentiful Rh^+ ions exist at the surface of SiO_2-ZrO_2 and ZrO_2 supported catalysts, because ZrO_2 could stabilize Rh^+ ions. This result implies that there exists a strong interaction between Rh and ZrO_2 support, thus leading to relative decrease of the interaction between Rh and Mn.

On the other hand, according to some reports [2,5,29,33,45], the interaction between Rh and Mn could suppress the reduction of Rh species and promote the reduction of Mn species. Thus, the strength of Rh-Mn interaction of catalysts could be compared by the difference in reduction temperature between Rh and Mn species: the small width of temperature region between Rh and Mn oxides reduction peaks indicates a strong Rh-Mn interaction [8,33]. In the present work, it can be seen from Fig. 5 that the interaction between Rh and Mn on RML/SiO_2 was the strongest, and that on RML/ZrO_2 was the weakest. It is suggested that the catalytic property of Rh-Mn based catalysts is very sensitive to the strength of Rh-Mn interaction; and only with moderate interaction between Rh and Mn could improve catalytic property [8,33]. It was worthy to note that the interaction between Rh and Mn of catalysts supported on SiO_2-ZrO_2 mixed oxide was between that on RML/SiO_2 and RML/ZrO_2, which exhibited better catalytic activity toward C_2-oxygenates. This result agrees well with that obtained by our previous work [27,46] and Chen et al. [8].

3.7. TPSR and CO-TPD study

As known that during the process of CO hydrogenation, the formation of CH_4 contains two procedures that is CO dissociation and then hydrogenation to form CH_4. Thus, the profile of CH_4 formation indirectly indicates the ability of CO dissociation related to the temperature of CH_4 formation and that of hydrogenation correlated with the peak intensity of CH_4 formation [29]. As shown in Fig. 6, compared with RML/SiO_2, CH_4 could be formed at lower temperatures on catalysts supported on ZrO_2 and SiO_2-ZrO_2 mixed oxides, indicating that RML/ZrO_2 and RML/SiO_2-ZrO_2 could improve the

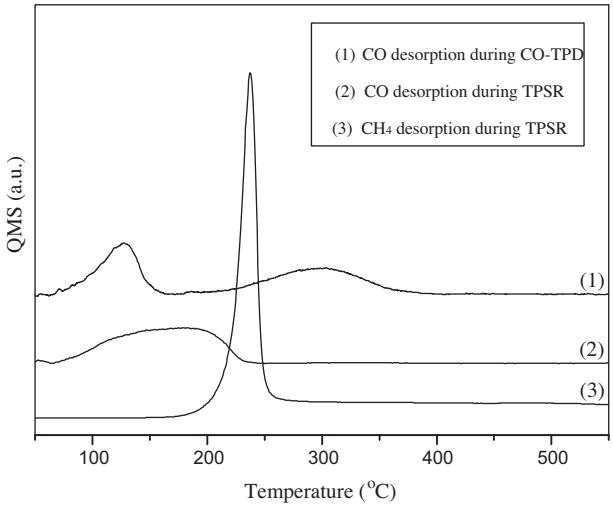

Fig. 7. Comparison of desorption products for TPD and TPSR.

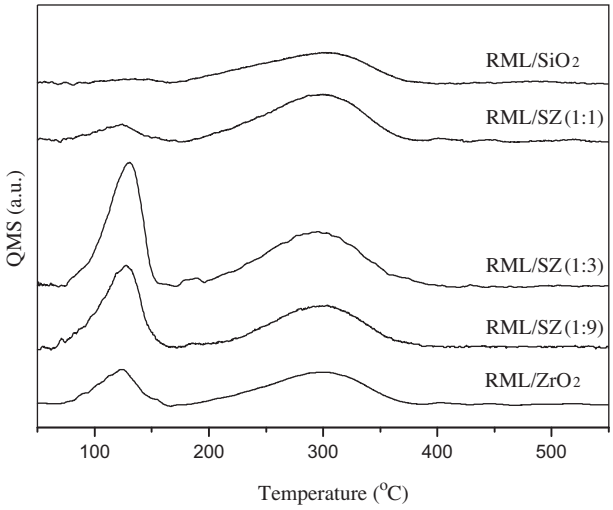

Fig. 8. CO-TPD-MS spectra of different catalysts.

ability of CO dissociation and thus increase the rate of CO conversion [47], which agreed with the result from FT-IR.

Chen et al. [48] argued that CO dissociation followed by hydrogenation into CH_x was interrelated with the activity of catalysts; moreover, CH_x hydrogenation into CH_4 and CH_x carbonylation as the precursor of C_2-oxygenates was a competing reaction. As shown in Fig. 6, the CH_4 peak intensity of catalysts increased in the order: RML/SiO_2 < RML/ZrO_2 < RML/SZ(1:9) < RML/SZ(1:3) < RML/SZ(1:1), in which RML/SZ(1:3) remains mediocre with medium capability of hydrogenation. Therefore, high activity and selectivity of C_2-oxygenates were obtained on RML/SZ(1:3), for its excellent ability of CO dissociation and moderate ability of hydrogenation [20].

Fig. 7 shows the profiles of CH_4 formation during TPSR and CO desorption during TPD and TPSR on RML/SZ(1:9). As seen from curve (1) in Fig. 7, there are two CO desorption peaks that correspond to weakly and strongly adsorbed CO, respectively [33]. Compared with curve (3), it was found that the weakly adsorbed CO desorbed completely before CO hydrogenation. From curves (2) and (3) in Fig. 7, it can be seen that quantities of CO that may correspond to weakly adsorbed CO desorbed before CO hydrogenation, and the intensity of CH_4 peak reached the maximum while CO desorbed completely. These results indicated that the weakly adsorbed CO dominantly desorbed before hydrogenation and only the strongly adsorbed CO could be hydrogenated, which was also suggested by other researchers [2,49]. Thus, it can be concluded that the catalytic activity is associated closely with the amount of strongly adsorbed CO [50]. On the other hand, the weakly adsorbed CO is suggested to be associated closely with the selectivity of C_2-oxygenates [50]. Increase of the relative proportion of activity sites for nondissociative CO adsorption implied more activity sites for CO insertion, which could improve the selectivity toward C_2-oxygenates.

The profiles of CO desorption on various catalysts are shown in Fig. 8. As seen, there are two CO desorption peaks on all the catalysts, which could correspond to weakly and strongly adsorbed CO, respectively. Peaks in Fig. 8 are processed using origin 7.0 and the peak areas are summarized in Table 4. It can be found that the amount of strongly adsorbed CO increased in the order of RML/SiO_2 < RML/ZrO_2 < RML/SZ(1:9) < RML/SZ(1:1) < RML/SZ(1:3), the same order as the catalytic activity. Moreover, the percentage of weakly adsorbed CO increased in the order of RML/SiO_2 < RML/SZ(1:1) < RML/ZrO_2 < RML/SZ(1:3) < RML/SZ(1:9), which agreed well with the selectivity of C_2-oxygenates of catalysts. These results well illustrate the specific effects of the strongly adsorbed CO and the weakly adsorbed CO played on the catalytic performance.

Table 4
Analysis for peak area of spectra in Fig. 8.

Catalyst	A_1[a] (a.u.)	A_2[b] (a.u.)	$A_1/(A_1+A_2)$
RML/SiO_2	4.2	71.8	0.06
RML/SZ(1:1)	16.5	99.7	0.14
RML/SZ(1:3)	96.4	118.9	0.45
RML/SZ(1:9)	74.9	87.7	0.46
RML/ZrO_2	31.6	72.3	0.30

[a] Low temperature peak area.
[b] High temperature peak area.

4. Conclusions

Compared with RML/SiO_2, CO conversion over RML/ZrO_2 did not improve evidently; however, its C_2-oxygenates selectivity improved notably. It is striking that Rh-Mn-Li supported on SiO_2-ZrO_2 mixed oxide improved not only the CO conversion but also the C_2-oxygenates selectivity. Results from FT-IR indicated that ZrO_2 and SiO_2-ZrO_2 mixed oxide stabilized Rh^+ ions, leading to more activity sites for CO insertion, namely the nondissociative CO adsorption, which was also confirmed by the results from XPS and CO-TPD. Moreover, a new adsorbed CO species, in which C-O weakened, were obtained on ZrO_2 and SiO_2-ZrO_2 supported catalysts, which contributed to CO dissociation. Results from H_2 and CO uptakes and FT-IR indicated that Rh dispersion on catalysts increased in the order of RML/SiO_2 < RML/ZrO_2 < RML/SZ(1:9) < RML/SZ(1:1) < RML/SZ(1:3). Increase of Rh dispersion implied more activity sites for CO dissociation and CO insertion, so that catalytic activity toward C_2-oxygenates synthesis increased in the same order. Results from TPSR of chemisorbed CO indicated that the ability of CO dissociation improved over SiO_2-ZrO_2 supported catalysts indeed, and moderate ability of hydrogenation was also conductive to increase the selectivity toward C_2-oxygenates. On the other hand, the moderate interaction of Rh-Mn over SiO_2-ZrO_2 mixed oxide supported catalysts also improved the catalytic properties.

Acknowledgments

The authors gratefully acknowledge financial support from the Science and Technology Commission of Shanghai Municipality

(08520513600) and Leading Academic Discipline Project of Shanghai Education Committee (J51503). The helpful suggestions for the revision of the manuscript provided by the anonymous reviewers are also gratefully acknowledged.

References

[1] R. Burch, M.I. Petch, Appl. Catal. A: Gen. 88 (1992) 39–60.
[2] H.M. Yin, Y.J. Ding, H.Y. Luo, H.J. Zhu, D.P. He, J.M. Xiong, L.W. Lin, Appl. Catal. A: Gen. 243 (2003) 155–164.
[3] R.P. Underwood, A.T. Bell, J. Catal. 111 (1988) 325–335.
[4] V. Subramani, S.K. Gangwal, Energy Fuels 22 (2008) 814–839.
[5] H.Y. Luo, P.Z. Lin, S.B. Xie, H.W. Zhou, C.H. Xu, S.Y. Huang, L.W. Lin, D.B. Liang, P.L. Yin, Q. Xin, J. Mol. Catal. A: Chem. 122 (1997) 115–123.
[6] S.C. Chuang, J.G. Goodwin Jr., I. Wender, J. Catal. 95 (1985) 435–446.
[7] M.A. Haider, M.R. Gogate, R.J. Davis, J. Catal. 261 (2009) 9–16.
[8] W.M. Chen, Y.J. Ding, H.Y. Luo, L. Yan, T. Wang, Z.D. Pan, H.J. Zhu, Chin. J. Appl. Chem. 22 (2005) 470–474.
[9] Y. Wang, H.Y. Luo, D.B. Liang, X.H. Bao, J. Catal. 196 (2000) 46–55.
[10] X.H. Mo, J. Gao, J.G. Goodwin Jr., Catal. Today 147 (2009) 139–149.
[11] H.Y. Luo, W. Zhang, H.W. Zhou, S.Y. Huang, P.Z. Lin, Y.J. Ding, L.W. Lin, Appl. Catal. A: Gen. 214 (2001) 161–166.
[12] J. Gao, X. Mo, A.C. Chien, W. Torres, J.G. Goodwin Jr., J. Catal. 262 (2009) 119–126.
[13] W.M. Chen, Y.J. Ding, D.H. Jiang, Z.D. Pan, H.Y. Luo, Catal. Lett. 104 (2005) 177–180.
[14] D.H. Jiang, Y.J. Ding, Z.D. Pan, W.M. Chen, H.Y. Luo, Catal. Lett. 121 (2008) 241–246.
[15] X.H. Mo, J. Gao, N. Umnajkaseam, J.G. Goodwin Jr., J. Catal. 267 (2009) 167–176.
[16] Y. Wang, J. Li, W. Mi, React. Kinet. Catal. Lett. 76 (2002) 141–150.
[17] P. Gronchi, E. Tempesti, C. Mazzocchia, Appl. Catal. A: Gen. 120 (1994) 115–126.
[18] A. Frydman, D.G. Castner, C.T. Campbell, M. Schmal, J. Catal. 188 (1999) 1–13.
[19] A. Trunschke, H. Ewald, H. Meissner, S. Marengo, S. Martinengo, F. Pinna, L. Zanderighi, J. Mol. Catal. 74 (1992) 365–377.
[20] L.P. Han, D.S. Mao, J. Yu, Q.S. Guo, G.Z. Lu, Catal. Commun. 23 (2012) 20–24.
[21] Z. Dang, B.G. Anderson, Y. Amenomiya, B.A. Morrow, J. Phys. Chem. 99 (1995) 14437–14443.
[22] T. Lei, J.S. Xu, Y. Tang, W.M. Hua, Z. Gao, Appl. Catal. A: Gen. 192 (2000) 181–188.
[23] M. Ichikawa, Bull. Chem. Soc. Japan 51 (1978) 2273–2277.
[24] T. Nakatsuji, T. Yamaguchi, N. Sato, H. Ohno, Appl. Catal. B: Environ. 85 (2008) 61–70.
[25] J.J. Wang, Q.H. Zhang, Y. Wang, Catal. Today 171 (2011) 257–265.
[26] J. Yu, D.S. Mao, L.P. Han, Q.S. Guo, G.Z. Lu, Catal. Commun. 24 (2012) 25–29.
[27] J. Yu, D.S. Mao, L.P. Han, Q.S. Guo, G.Z. Lu, Fuel Process. Technol. 106 (2013) 344–349.
[28] Z.L. Fan, W. Chen, X.L. Pan, X.H. Bao, Catal. Today 147 (2009) 86–93.
[29] G.C. Chen, C.Y. Guo, X.H. Zhang, Z.J. Huang, G.Q. Yuan, Fuel Process. Technol. 92 (2011) 456–461.
[30] C. Dell'Agnol, A. Gervasini, F. Morazzoni, F. Pinna, G. Strukul, L. Zanderighi, J. Catal. 96 (1985) 106–114.
[31] M. Ichikawa, T. Fukushima, J. Phys. Chem. 89 (1985) 1564–1567.
[32] Y.Y. Liu, K. Murata, M. Inaba, I. Takahara, K. Okabe, Catal. Today 164 (2011) 308–314.
[33] W.M. Chen, Y.J. Ding, D.H. Jiang, Z.D. Pan, H.Y. Luo, J. Nat. Gas Chem. 14 (2005) 199–206.
[34] S.S.C. Chuang, S.I. Pien, J. Catal. 135 (1992) 618–634.
[35] M. Kawai, M. Uda, M. Ichikawa, J. Phys. Chem. 89 (1985) 1654–1656.
[36] H. Ngo, Y.Y. Liu, K. Murata, React. Kinet. Mech. Catal. 102 (2011) 425–435.
[37] M. Ichikawa, T. Fukushima, J. Chem. Soc. Chem. Commun. 6 (1985) 321–323.
[38] M. Ojeda, M.L. Granados, S. Rojas, P. Terreros, F.J. García-García, J.L.G. Fierro, Appl. Catal. A: Gen. 261 (2004) 47–55.
[39] R. Burch, M.I. Petch, Appl. Catal. A: Gen. 88 (1992) 77–99.
[40] A. Egbebi, V. Schwartz, S.H. Overbury, J.J. Spivey, Catal. Today 149 (2010) 91–97.
[41] H. Kusama, K. Okabe, K. Sayama, H. Arakawa, Catal. Today 28 (1996) 261–266.
[42] V. Schwartz, A. Campos, A. Egbebi, J.J. Spivey, S.H. Overbury, ACS Catal. 1 (2011) 1298–1306.
[43] P. Reyes, I. Concha, G. Pecchi, J.L.G. Fierro, J. Mol. Catal. A: Chem. 129 (1998) 269–278.
[44] D.H. Jiang, Y.J. Ding, Z.D. Pan, X.M. Li, G.P. Jiao, J.W. Li, W.M. Chen, H.Y. Luo, Appl. Catal. A: Gen. 331 (2007) 70–77.
[45] G.C. Chen, X.H. Zhang, C.Y. Guo, G.Q. Yuan, Comptes Rendus Chimie 13 (2010) 1384–1390.
[46] J. Yu, D.S. Mao, L.P. Han, Q.S. Guo, G.Z. Lu, J. Mol. Catal. A: Chem. 367 (2013) 38–45.
[47] W.M.H. Sachtler, M. Ichikawa, J. Phys. Chem. 90 (1986) 4752–4758.
[48] W.M. Chen, Y.J. Ding, D.H. Jiang, G.P. Jiao, H.J. Zhu, Z.D. Pan, H.Y. Luo, Chin. J. Catal. 27 (2006) 999–1004.
[49] K. Fujimoto, M. Kameyama, J. Kunugi, J. Catal. 61 (1980) 7–14.
[50] D.H. Jiang, Y.J. Ding, Y. Lv, H.J. Zhu, W.M. Chen, T. Wang, L. Yan, H.Y. Luo, Chin. J. Catal. 30 (2009) 697–703.